(Received 28 March 2024, Accepted 28 May 2024, Scheduled 5 July 2024)

Analysis of a Triple band MIMO Antenna for Sub-6 GHz Applications

Govardhani Immadi[1,*], Madhavareddy Venkata Narayana[1], Ambati Navya[1], Aovuthu Sree Madhuri[2], Burra Vamsi Krishna[1], and Marri Venkata Siva Gopi[1]

[1]*Department of ECE, KLEF, Vaddeswaram, Guntur, Andhra Pradesh, India*
[2]*Department of Electronics & Communication Engineering, Rashtreeya Vidyalaya College of Engineering, Bangalore, India*

ABSTRACT: A triple band MIMO antenna is designed and analysed at sub-6 GHz for 5G applications on an FR-4 substrate. This paper contains the transition of an antenna from a simple microstrip antenna to the proposed defected L-shaped microstrip patch antenna, which comprises single, 2-element MIMO, and 4-element MIMO antennas with permittivity of 4.3, and the dimensions of those antennas are $60 \times 60\,\text{mm}^2$, $60 \times 120\,\text{mm}^2$, and $120 \times 120\,\text{mm}^2$ correspondingly. These antennas resonate at three resonant frequencies which are 3 GHz, 4.1 GHz and 5.2 GHz under sub-6 GHz. HFSS has been used to design these antennas and to obtain the parameters like S-parameters, gain, VSWR, and MIMO parameters like ECC, DG, TARC, and MEG. At those resonant frequencies, single element antenna has S_{11} of -26.83 dB, -20.06 dB, and -19.16 dB; two element MIMO antennas have S_{11} of -22.7 dB, -40.09, and -20.54 dB; and quad element MIMO antennas have S_{11} of -15 dB, -24.8 dB, and -22.7 dB. The overall antenna gains are 2.5061 dBi, 3.1903 dBi, and 4.2989 dBi for single, 2-port, and 4-port MIMO antennas. This antenna is well suited for a range of applications including FWA systems that utilize 3 GHz frequency, Smart Cities and connected vehicles that rely on 4.1 GHz, and high-bandwidth activities such as video streaming, cloud computing, and mission-critical communications that require 5.2 GHz. Additionally, it can support future developments in both 5G and Wi-Fi technologies.

1. INTRODUCTION

Intelligent antenna technology and diversity technology for wireless communication are the ancestors of multiple-input multiple-output (MIMO) technology. It combines the advantages and characteristics of multiple-input single-output (MISO) and single-input multiple-output (SIMO); therefore, it has both [1, 2]. Without increasing the bandwidth or transmitted power, it can exponentially increase the speed and quality of the effective signal transmission [3, 4]. The growth of mobile communications in recent times has had a crucial impact on both social and economic growth. Therefore, 5G technology becomes the standard for the generation of 2020. A new technology, 5G offers both evolutionary and revolutionary services. It is important to bear in mind that 5G technology will bring forth new challenges and necessitate the establishment of development restrictions [5, 6]. In many of the domains like agriculture, healthcare, defence, and other industries, the 5G technology has evolved and leads to development in people's lives [7–9].

Several authors have undertaken in-depth research on the design of MIMO multi-element antennas for 5G applications, including slot antennas, dual-polarised antennas, and structured monopoles, according to the literature. The essential technology for 5G communication also includes cognitive radio; however, designing an antenna that uses both CR (cognitive radio) and MIMO is a difficult issue [6]. The foundation of 4G wireless communication systems has been shown to be MIMO technology and beyond in order to transfer the data to satisfy the rising demand [10, 12]. When small printed circuit boards (PCBs) are designed for efficient transmission, various MIMO antennas have been designed [11, 12]. To reduce the undesired mutual coupling, several isolation approaches have been published in recent years [13–15]. In [13], defective ground plane's rectangular slots and two microstrip lines are very useful for the reduction of the mutual coupling. In order to reduce the coupling between antenna and surrounding components, [14] uses a vertical patch. With no need to increase transmitting power or bandwidth, the MIMO concept can significantly improve data rate, range, and reliability by reducing the impacts of multipath fading. The deployment of several antennas inside a handheld device, however, is a difficult operation due to the restricted space available. The radiating elements are subject to strong internal coupling because of closely spaced operating frequencies. Consequently, a small, effective MIMO antenna that has excellent isolation, minimal mutual coupling, and the ability to block undesired frequency bands is required [16]. Especially for low frequency technology, increasing the isolation between nearby MIMO antennas is a difficult issue. A variety of methods have been employed to improve the isolation between antennas. Antenna orientation [17, 18], the addition of decoupling structures [18, 19], ground plane modifications [18, 20–22], lumped component filters [23], neutralisation strips, the addition of resonating structures close to the

* Corresponding author: Govardhani Immadi (govardhanee_ec@kluniversity.in).

TABLE 1. Dimensions for defected L-shaped microstrip patch antenna.

S. No	Variables	Values (mm)	S. No	Variables	Values (mm)
1	Patch Length (L_P)	29.4	15	Radius of circle (R_1)	1.5
2	Patch Width (W_P)	38	16	Length (L_6)	40
3	Feedline length (L_F)	15.3	17	Width (W_6)	3
4	Feedline width (W_F)	3	18	Length (L_7)	3
5	Length (L_1)	10	19	Width (W_7)	41
6	Width (W_1)	12	20	Length (L_8)	3
7	Length (L_2)	2	21	Width (W_8)	8
8	Width (W_2)	8	22	Length (L_9)	25
9	Length (L_3)	34	23	Width (W_9)	3.5
10	Width (W_3)	1	24	Length (L_{10})	3.5
11	Length (L_4)	1	25	Width (W_{10})	23.5
12	Width (W_4)	23.5	26	Length (L_{11})	3.5
13	Length (L_5)	1	27	Width (W_{11})	4
14	Width (W_5)	4	28	Radius of Circle (R_2)	2

antennas [24], the introduction of resonating structures in the antennas [17], and the usage of metamaterials [25–27] are a few reported techniques. A slotted planar antenna has been designed, simulated, and tested for 5G applications [28]. A 4-elemental MIMO antenna has been designed for ISM band applications, and various MIMO parameters like envelope correlation coefficient (ECC), diversity gain (DG), and total active reflection coefficient (TARC) were measured by using Vector Network Analyzer (VNA) [29]. A new broadband MIMO antenna has been designed for sub-6 GHz 5G applications [30]. A novel dipole antenna has been designed with metallic sheets for ultra-high frequency (UHF) and very high frequency (VHF) applications [31]. A reflector array antenna has been designed at millimetric band for on the move applications [32]. Using CST Microwave Studio, a substrate integrated frequency selective surface antenna has been designed for Internet of Things applications [33]. With $ka < 1$, a Low-Profile Electrically Small Antenna with a Circular Slot has been designed for applications involving global positioning systems [34]. Different dielectric resonator antennas have been designed for different wireless communication applications, including a small multiband hybrid rectangular dielectric resonator antenna (DRA) [35]. For radio frequency identification (RFID) applications, a small, electrically compact antenna with split ring resonators has been developed [36]. For RFID applications, a low-profile dual-band electrically small antenna has been developed [37]. For RFID applications, a tiny electronically serrated rectangular patch antenna has been developed [38]. In order to design two and four elemental MIMO antennas, the optimisation of a single element antenna design is followed by the replica of that antenna geometry in both the horizontal and vertical orientations. ECC and DG were used to measure S-parameters and other MIMO antenna parameters, and all of the results are in line with the values reported in [39].

The aim is to design a MIMO antenna suitable for 5G applications within the sub-6 GHz frequency range. Such antennas have various applications in 5G technologies [7–9] such as smart homes, industrial automation, agriculture, surveillance, and medical care. The obtained resonating frequencies for the designed antenna are 3 GHz, 4.1 GHz, and 5.2 GHz. The country that accepts the 5G communication network's frequency band, including 3 GHz, is the USA (3–3.55 GHz) [28].

2. DESIGN METHODOLOGY

This design methodology covers various stages involved in designing a MIMO antenna, providing detailed information on its design, the materials used in its design, as well as its dimensions. The article also presents a parametric analysis of the antenna at each stage of its development, including an evaluation of parameters such as S_{11}, gain, VSWR, and ECC.

The rectangular microstrip antenna is fed by a microstrip transmission line which has a full ground and characteristic impedance of 50 Ω. The dimensions of the patch antenna are calculated for 5G communication applications at sub-6 GHz, and the antenna occupies a space of $29.4 \times 38 \times 1.6\,\text{mm}^2$. Two rectangular patches with L-shaped slots measuring $10 \times 2\,\text{mm}^2$ and $2 \times 8\,\text{mm}^2$ are subtracted from the microstrip patch for better results of return loss and other antenna parameters. Complementary SRRs were used in the design to eliminate the resonant frequencies beyond 6 GHz. Table 1 represents the measurements of the defected L-shaped microstrip antenna, and its design is shown in Figure 1(a).

Figure 2 presents the iterative design of a defected L-shaped microstrip patch antenna. The antenna was designed to work for applications in sub-6 GHz band at 3 GHz, 4.1 GHz, and 5.2 GHz. However, the antenna does not resonate at those frequencies, indicating that adjustments to the design were needed to achieve the desired results for those specific applications. Here, four rectangles are united together in which two of them have the same dimensions and are placed opposite to each other. One of the rectangles has $34 \times 1\,\text{mm}^2$ dimensions and the other one with $1 \times 23.5\,\text{mm}^2$ dimensions, and we have subtracted a small rectangle from the patch with the dimensions of

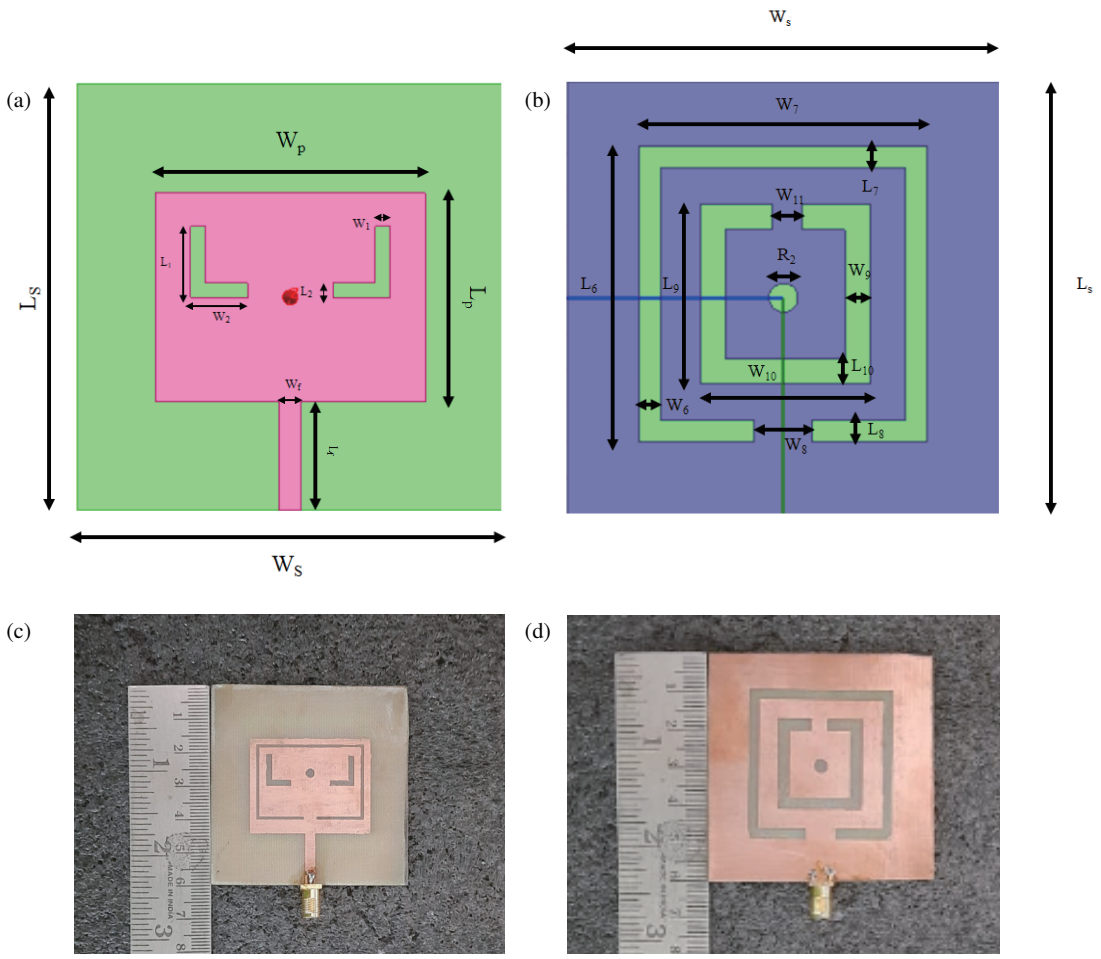

FIGURE 1. Defected L-shaped MPA. (a) Top plane. (b) Bottom plane. (c) Photograph from top view. (d) Photograph from bottom view.

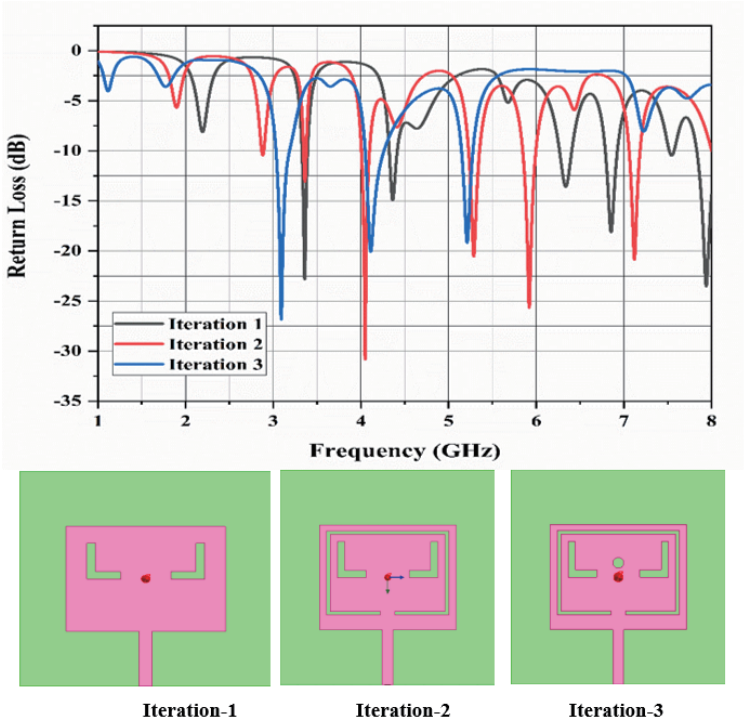

FIGURE 2. Evolution of the defected L-shaped microstrip patch antenna.

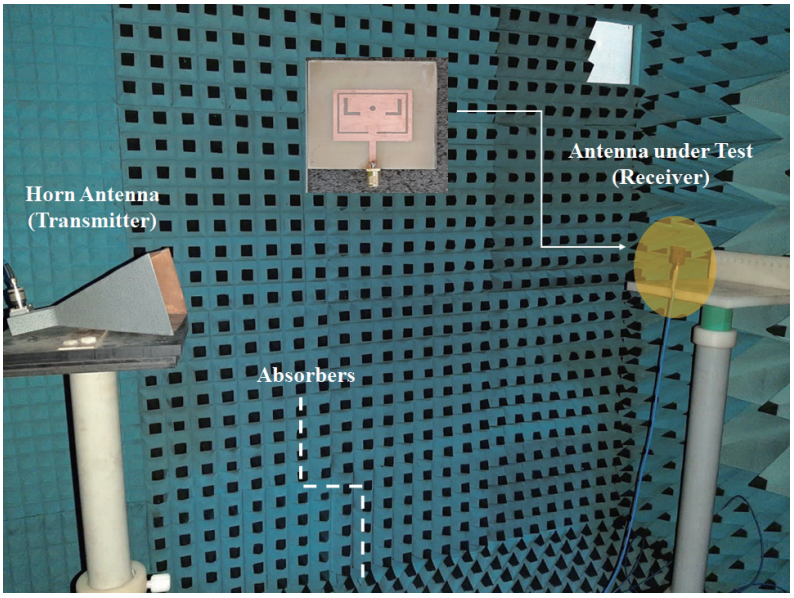

FIGURE 3. Radiation pattern measurement of defected L-shaped microstrip patch antenna utilising anechoic chamber.

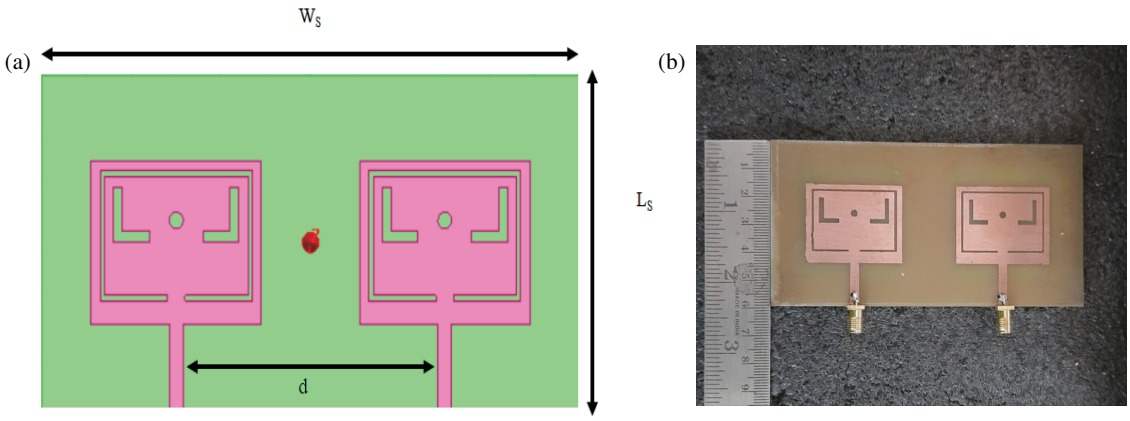

FIGURE 4. Dual-element defected L-shaped microstrip patch MIMO antenna. (a) Simulated. (b) Manufactured design.

$1\times4\,\text{mm}^2$. The second iteration's results indicate that the return loss of the antenna has undergone changes at various frequencies. At 3 GHz, it has shifted from -22.82 dB to -13.08 dB, at 4.1 GHz and at 5.2 GHz return loss of -30.8 dB and at 5.9 GHz return loss of -20.54 dB from -25.62 dB. While these frequencies may be suitable for different applications, they do not meet the desired requirements. Thus, further modifications are necessary to attain the desired results. During the third iteration, the rectangular patch is modified by removing a circle with radius of 1.5 mm, which is denoted as R_1. In the ground, we have utilized complementary SRRs with dimensions of $41\times3\,\text{mm}^2$ and $3\times40\,\text{mm}^2$. Again, the ground is modified by removing a circle with radius of 2 mm, which is denoted as R_2. In the third iteration, a 3 GHz resonance with -26.83 dB return loss, 4.1 GHz resonance with -19.16 dB return loss and 5.2 GHz resonance with 20.06 dB return loss are obtained. Since this design meets all the requirements of the proposed idea, it is deemed to be the final design proposal. Figure 3 presents the measurement setup of an anechoic chamber which can be used to measure radiation pattern and gain with the utilization of MS2037C Anritsu Combinational Analyser.

To design a dual-element defected L-shaped microstrip patch MIMO antenna, the single element antenna is duplicated along the horizontal axis. Multiple elements in the MIMO antenna will provide multiple data streams to transmit and receive large amount data simultaneously. The signals are received from multiple directions, which improves the signal quality and overall performance. So, to attain these parameters, a MIMO antenna technology is the right choice. To achieve the spatial diversity seen in Figure 4, the inter-element distance between the two elements was kept at $\lambda/4$. The antenna's design is made more challenging because it was found that no further isolation techniques were needed. This dual-element antenna has a size of $60\times120\times1.6\,\text{mm}^3$. The simulated and fabricated

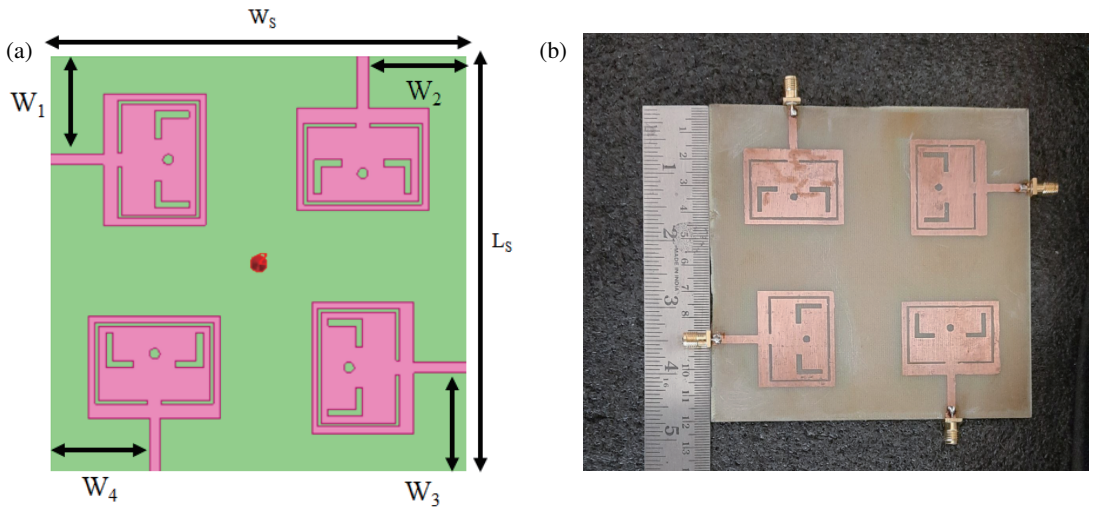

FIGURE 5. Quad-element defected L-shaped microstrip patch MIMO antenna. (a) Simulated design. (b) Manufactured design.

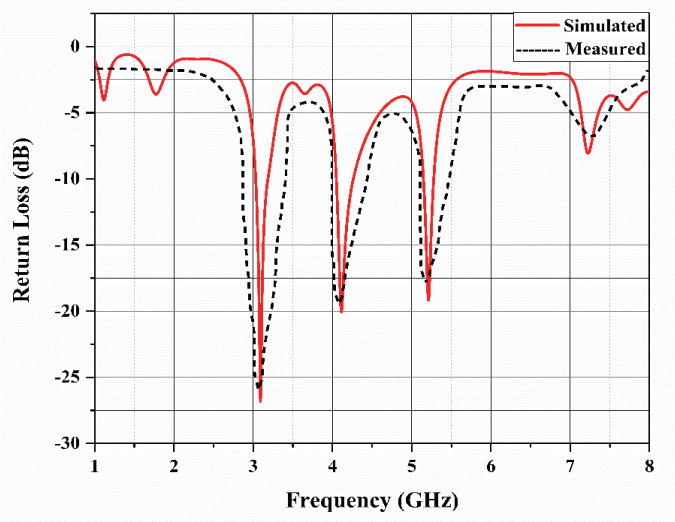

FIGURE 6. Simulated and measured S_{11} of the defected L-shaped MPA.

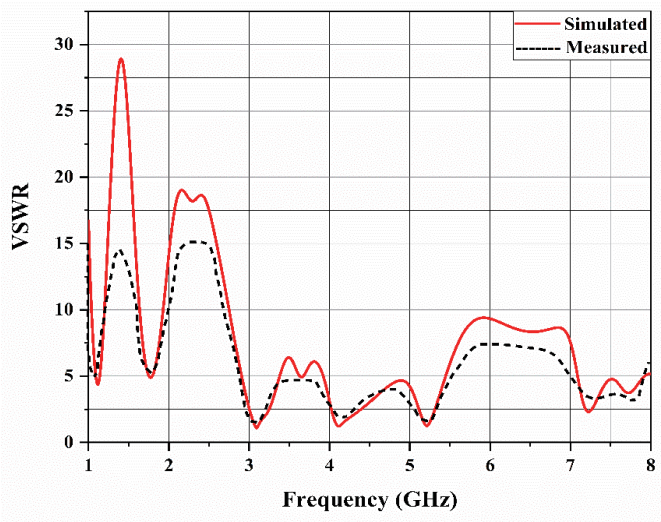

FIGURE 7. Simulated and measured VSWRs of the defected L-shaped microstrip patch antenna.

dual-element defected L-shaped microstrip patch MIMO antennas are represented in Figure 4. MPA is further modified by replicating two elements along the vertical-axis to obtain a four-element defected L-shaped microstrip patch MIMO antenna. The inter-element spacing of $\lambda/4$ has been maintained along x-axis and y-axis antenna elements. This four-element MIMO antenna occupies a size of $120 \times 120 \times 1.6\,\text{mm}^3$. Figure 5 presents the simulated and fabricated designs of the quad-element defected L-shaped microstrip patch MIMO antenna.

3. RESULTS & DISCUSSIONS

This section is separated into subsections that give a detailed explanation of the simulated results and the conclusions that can be made from the simulated outcomes.

3.1. Single-Element Defected L-Shaped Microstrip Patch Antenna

The final iteration antenna is manufactured by utilising FR4 epoxy material as represented in Figure 1. The radiating bottom and top planes are connected by using the substrate, which are attached by utilising the SMA connector.

The analysis of measured and simulated results of S_{11} parameters was the only goal in fabricating the design prototype. The prototype resonates at 3 GHz. The return loss was -24.93 dB, and at 4.1 GHz it was -19.51 dB and at 5.2 GHz with -17.83 dB return loss. The simulated antenna resonates at 3 GHz with the return loss of -26.83 dB, at 4.1 GHz with -20.06 dB return loss, and at 5.2 GHz with -19.16 dB return loss as shown in Figure 6. There is a minor variance in the results due to equipment's calibration level, connector losses, as well as the cable losses.

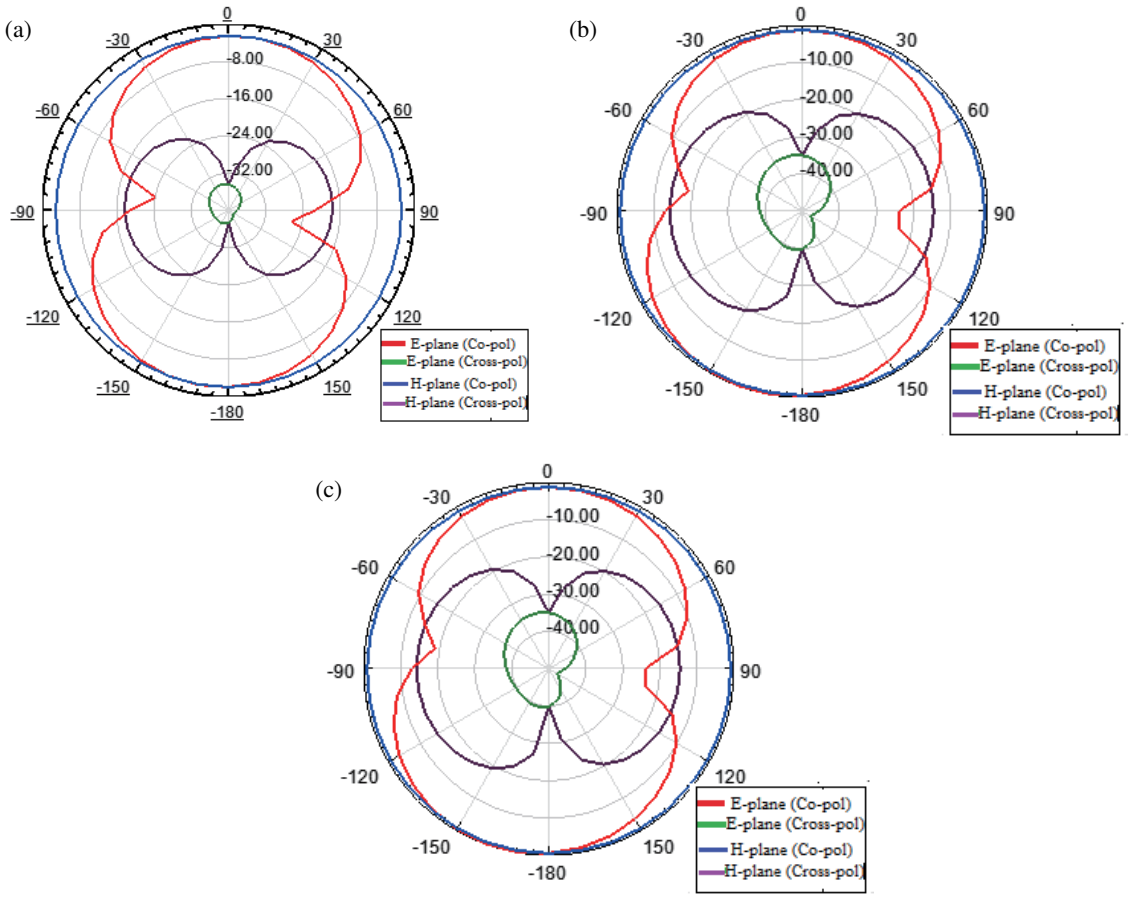

FIGURE 8. Simulated and measured radiation patterns of the single-element defected L-shaped microstrip patch antenna (a) at 3 GHz (b) at 4.1 GHz (c) at 5.2 GHz.

The range of 0–2 is required for the optimal value of VSWR. For the single element antenna, the observed and simulated VSWR values are 1.32 and 1.09 for 3 GHz, 1.6 and 1.22 for 4.1 GHz, and 1.53 and 1.22 for 5.2 GHz, respectively, shown in Figure 7. The antenna is placed in an anechoic chamber to measure the radiation pattern. Figure 8 illustrates the radiation pattern of the implemented design in E-plane and H-plane at 3 GHz, 4.1 GHz, and 5.20 GHz. In both the principal planes (E&H), there is good co-pol and cross-pol difference in broadside direction, i.e., more than 20 dB at all three frequency bands. It can be seen from Figure 8 that the radiation patterns in E- and H-planes are omnidirectional at the two resonant frequency bands. The presented model has good radiation properties. Figures 9(a), (b), and (c) show surface current distributions for 3 GHz, 4.1 GHz, and 5.2 GHz, respectively. The distribution of current on the antenna provides the insights of performance and efficiency of the antenna. From observing Figure 9, we can interpret that the electric current has been distributed symmetrically throughout the patch and the feedline, concluding that the antenna is efficient. Figure 10 presents the 3-dimensional gain of the single-element defected L-shaped microstrip patch antenna where a maximum gain of 2.5 dBi is observed.

3.2. Dual-Element Defected L-Shaped Microstrip Patch MIMO Antenna

The two main concerns for 5G are data throughput and accuracy. MIMO antenna technology is thought to be the optimal choice for improved performance. The MIMO antenna's numerous components will enable it to send and receive a significant quantity of data concurrently in various data streams. Signal quality and overall performance suffer as a result of the signals being received from various directions. MIMO antenna technology is the best option in order to achieve these criteria. The prototype of the dual-element defected L-shaped microstrip patch MIMO antenna is represented in Figure 4. This section examines the performance of a dual-element defected L-shaped microstrip patch MIMO antenna in terms of S_{11}, transmission coefficient, VSWR, radiation pattern, gain, and surface current distributions as well as other MIMO antenna parameters like ECC and DG. Figure 11 presents the simulated and fabricated S_{11} of the dual-element defected hexagonal-patch MIMO antenna. Figure 12 presents the simulated and fabricated S_{12} of the dual-element defected hexagonal-patch MIMO antenna.

Figure 13 displays all of the S-parameters, whereas Figure 11 displays the S_{11} results from the two-port MIMO antenna, and

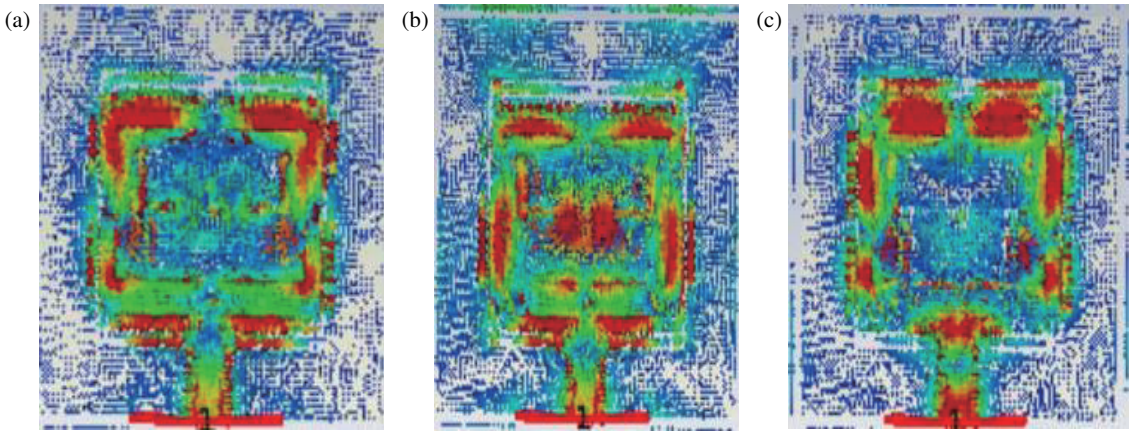

FIGURE 9. Surface current distribution of the single-element defected L-shaped microstrip patch antenna. (a) 3 GHz, (b) 4.1 GHz, (c) 5.2 GHz.

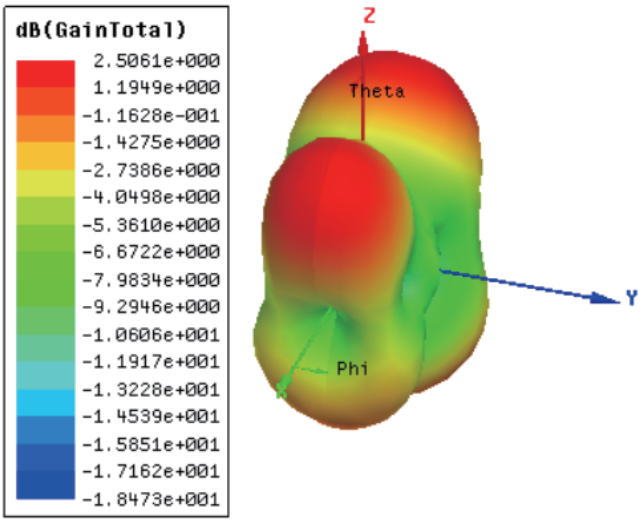

FIGURE 10. 3-dimensional gain of the single-element defected L-shaped microstrip patch antenna.

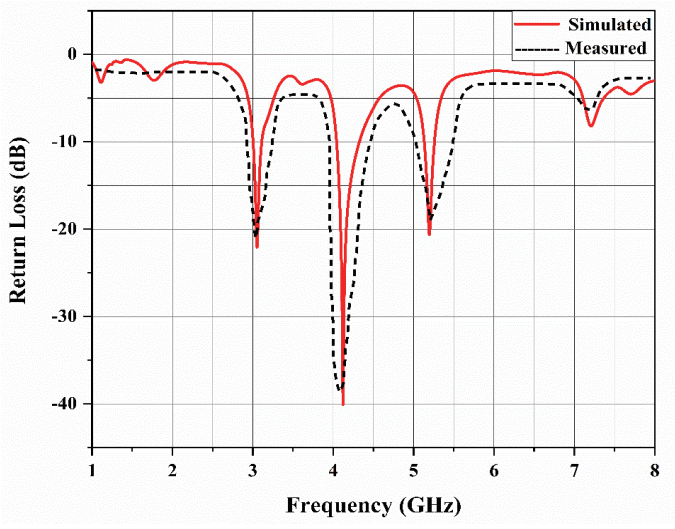

FIGURE 11. Simulated and measured S_{11} of the dual-element defected L-shaped microstrip patch MIMO antenna.

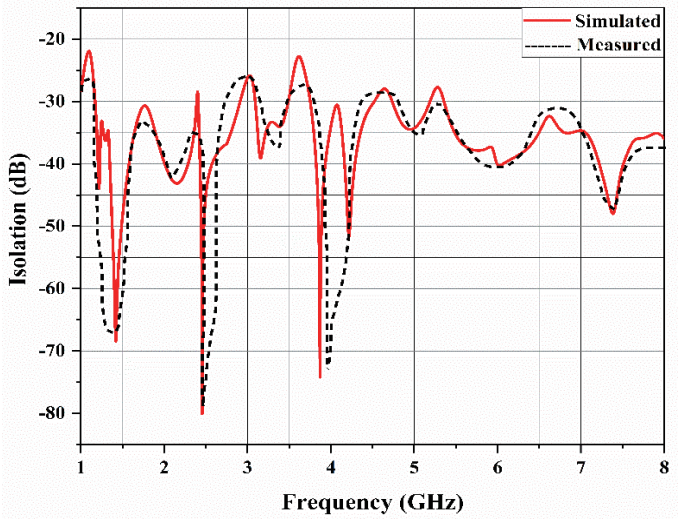

FIGURE 12. Simulated and measured S_{12} of the dual-element defected L-shaped microstrip patch MIMO antenna.

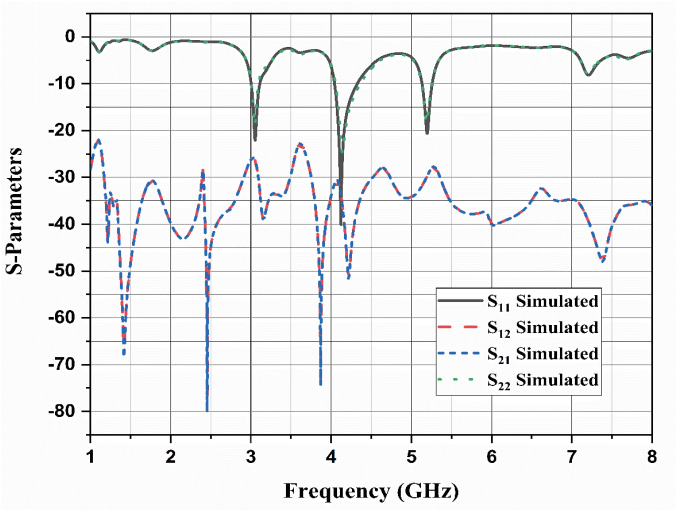

FIGURE 13. Simulated S-parameters of the dual-element defected L-shaped microstrip patch MIMO antenna.

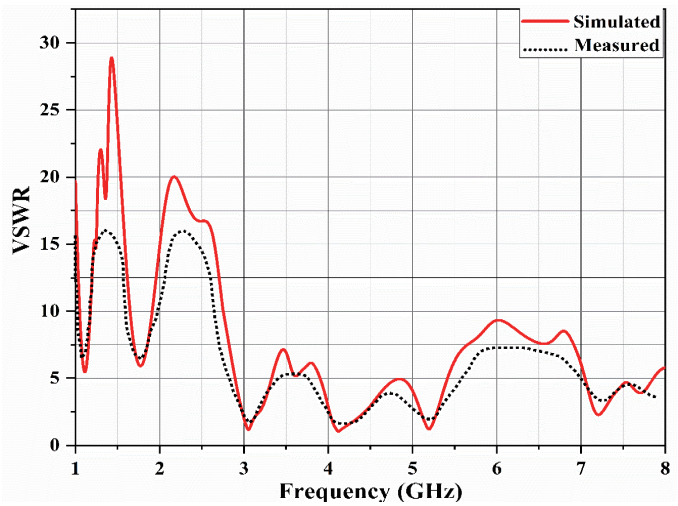

FIGURE 14. Simulated and measured VSWRs of the dual-element defected L-shaped microstrip patch MIMO antenna.

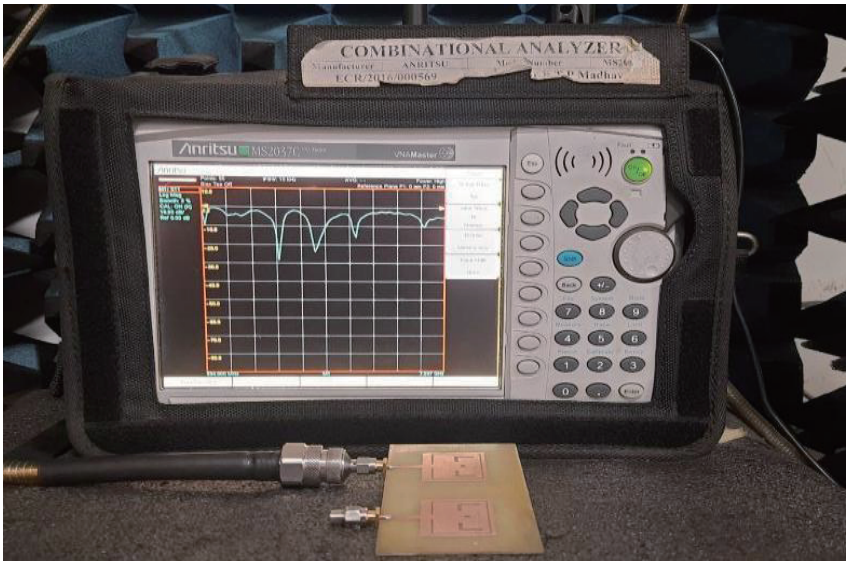

FIGURE 15. Measurement of S_{11} results by MS2037C anritsu combinational analyser.

Figure 12 shows the S_{21} results from the dual-port MIMO antenna. According to Figure 11's comparison of simulated and measured antennas, the simulated antenna resonates at 3 GHz with a return loss of -22.07 dB, 4.1 GHz with -40.09 dB return loss and at 5.2 GHz with -20.54 dB return loss, while the fabricated design resonates at 3 GHz with -28.8 dB return loss, 4.1 GHz with a return loss of -24.9 dB, and S_{11} findings for a two-port antenna in a combinational analyzer are shown in Figure 15. Figure 14 displays the VSWR findings. At 3 GHz, the simulated and measured VSWRs are 1.7 and 1.9; at 4.1 GHz, they are 1.02 and 1.41, respectively; and at 5.2 GHz, they are 1.2 and 1.51, respectively. This indicates that the antenna performs satisfactorily. Figures 16 and 17 show the two-port antenna's radiation pattern and surface current distribution, respectively, for 3 GHz, 4.1 GHz, and 5.2 GHz bands. The measured and simulated radiation patterns of two-port MIMO antenna are shown in Figure 16, which illustrates the radiation pattern of implemented design in E-plane and H-plane at 3 GHz, 4.1 GHz, and 5.20 GHz. In both the principal planes (E & H), there is good co-pol and cross-pol difference in broadside direction, i.e., more than 20 dB at all three frequency bands. It can be seen from Figure 16 that the radiation patterns in E- and H-planes are omnidirectional at the two resonant frequency bands. The presented model has good radiation properties. Figure 18 presents the 3D gain of the dual-element defected L-shaped MPA. Figure 17 presents the surface current distribution of the dual-element defected L-shaped MPA at three different resonant frequencies, 3 GHz, 4.1 GHz, and 5.2 GHz.

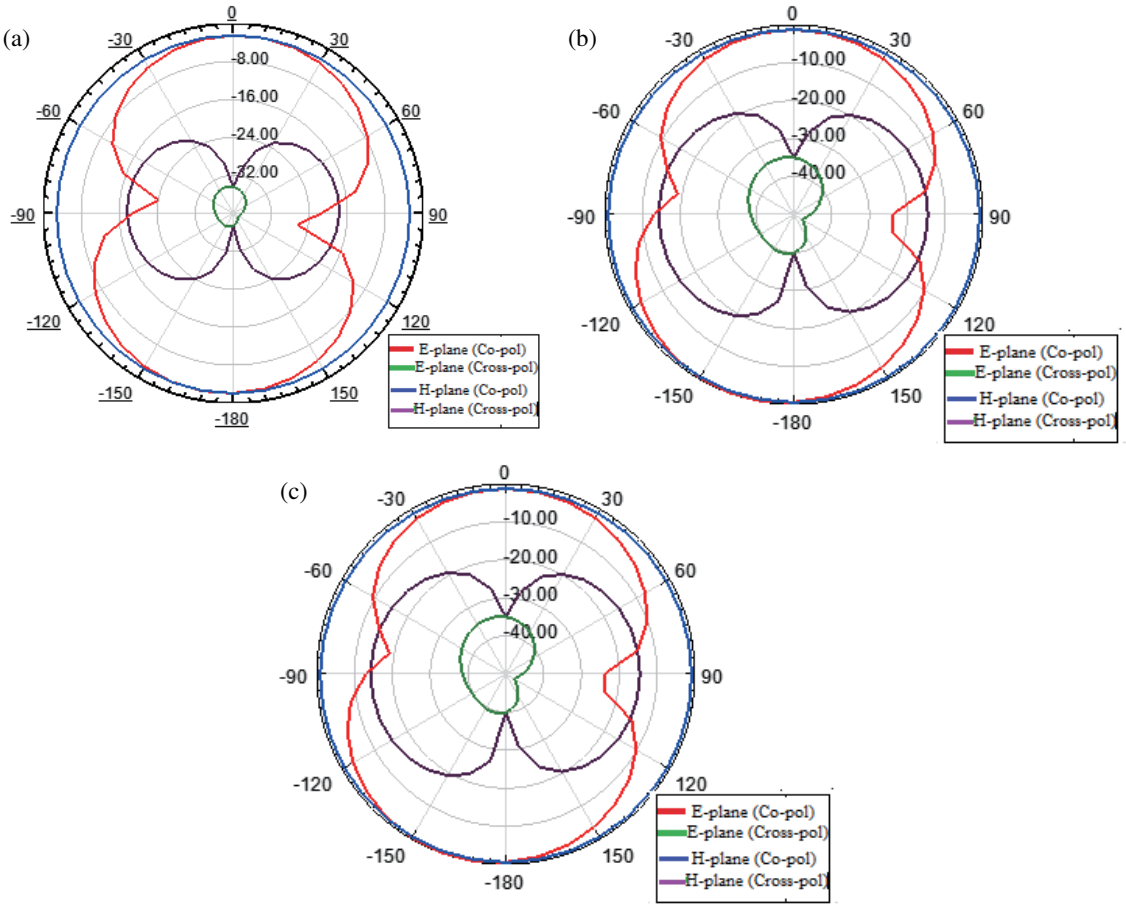

FIGURE 16. Simulated and measured radiation patterns of the dual-element defected L-shaped microstrip patch antenna (a) at 3 GHz (b) at 4.1 GHz (c) at 5.2 GHz.

3.3. Four-Element Defected L-Shaped Microstrip Patch MIMO Antenna

With further modifications, the antenna's two-port design is changed to a quad-port MIMO antenna. The quad-element MIMO antenna performance by means of S_{11}, transmission coefficient, VSWR, radiation pattern, gain, and J-surface distributions along with the other MIMO antenna parameters like ECC and DG is obtained in this section. The simulated and prototype designs resonate at a frequency of 3 GHz with -29.21 dB and -27.54 dB return loss, respectively, at 4.1 GHz frequency with -18.35 dB and -16.95 dB return loss, respectively, and at 5.2 GHz frequency with -22.57 dB and -21.81 dB return loss, respectively. Figure 19 presents the simulated and measured S_{11} of the quad-element defected L-shaped microstrip patch MIMO antenna. Figure 20 presents the simulated and measured S_{12} of the quad-element defected L-shaped microstrip patch MIMO antenna. From Figure 21, we interpret that the return loss at S_{11}, S_{22}, S_{33}, S_{44} at 3 GHz, 4.1 GHz, and 5.2 GHz are -15.77 dB, -25.72 dB, and -22.34 dB, respectively. The isolation coefficient at 3 GHz ranges from -25 dB to -36 dB; at 4.1 GHz it ranges from -29 dB to -37 dB; and for 5.2 GHz it ranges from -28 dB to -35 dB. In Figure 22, the VSWR of the simulated design at frequencies 3 GHz, 4.1 GHz, and 5.2 GHz are 1.28, 1.07, and 1.19, respectively, and VSWRs of the prototype at frequencies 3 GHz, 4.1 GHz, and 5.2 GHz are 1.32, 1.12, and 1.21, respectively. Figure 23 presents the measurement setup of the S-parameters and VSWR by utilising MS2037C Anritsu Combinational Analyser. The radiation patterns of Figure 24 display simulated and measured antennas at 3 GHz, 4.1 GHz, and 5.2 GHz. The four-port MIMO antenna's actual radiation and simulated patterns are shown in Figure 24, which illustrates the radiation patterns of implemented design in E-plane and H-plane at 3 GHz, 4.1 GHz, and 5.20 GHz. In both the principal planes (E&H), there is good co-pol and cross-pol difference in broadside direction, i.e., more than 20 dB at all three frequency bands. It can be seen from Figure 24 that the radiation patterns in E- and H-planes are omnidirectional at the two resonant frequency bands. The presented model has good radiation properties. Figure 25 presents the distribution of surface current on the antenna at each port. Figure 26 represents the 3D gain of the quad-element defected L-shaped microstrip patch MIMO antenna.

3.4. Analysis of MIMO Diversity Parameters

When the effectiveness of MIMO diversity parameters is measured, ECC and DG are used to guarantee that the designed antenna satisfies the specifications outlined in [15–19].

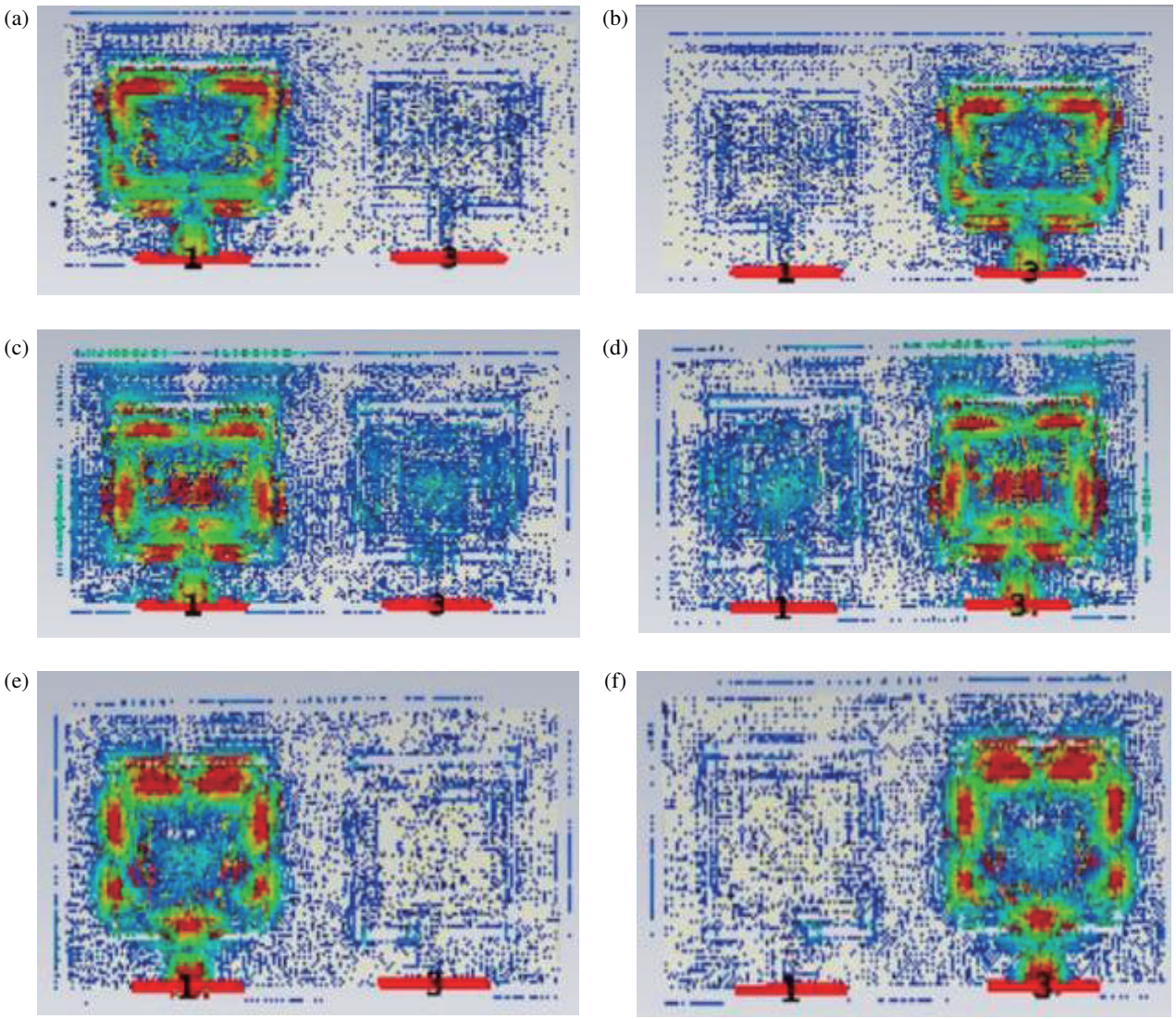

FIGURE 17. Surface current distribution of the dual-element defected L-shaped microstrip patch antenna. (a, b) 3.0 GHz, (c, d) 4.1 GHz, (e, f) 5.2 GHz.

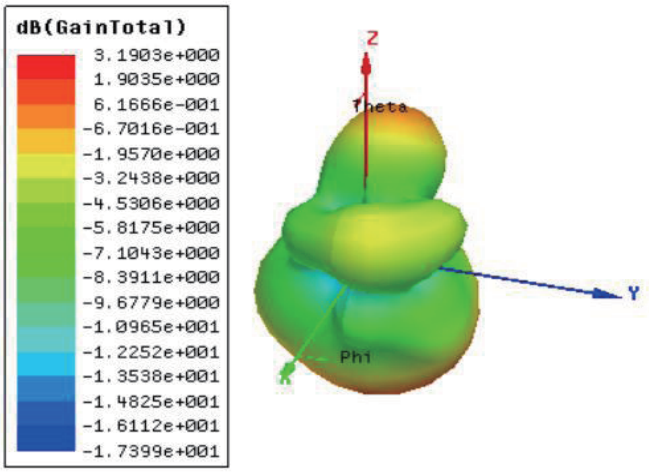

FIGURE 18. 3-dimensional gain of the single-element defected L-shaped microstrip patch antenna.

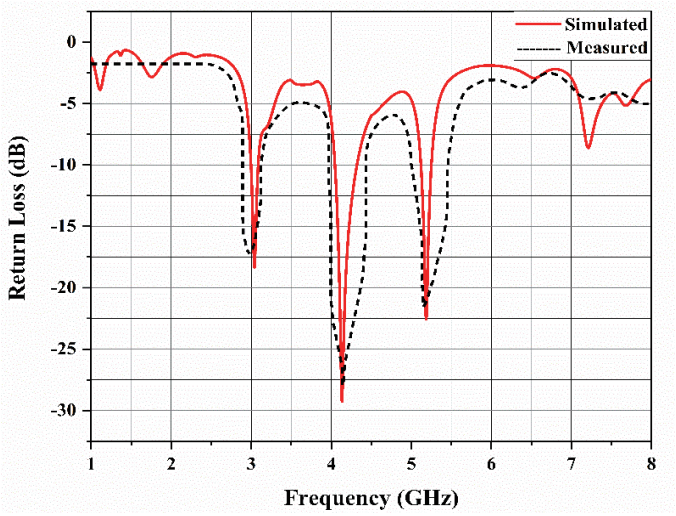

FIGURE 19. Simulated and measured S_{11} of the quad-element defected L-shaped microstrip patch MIMO antenna.

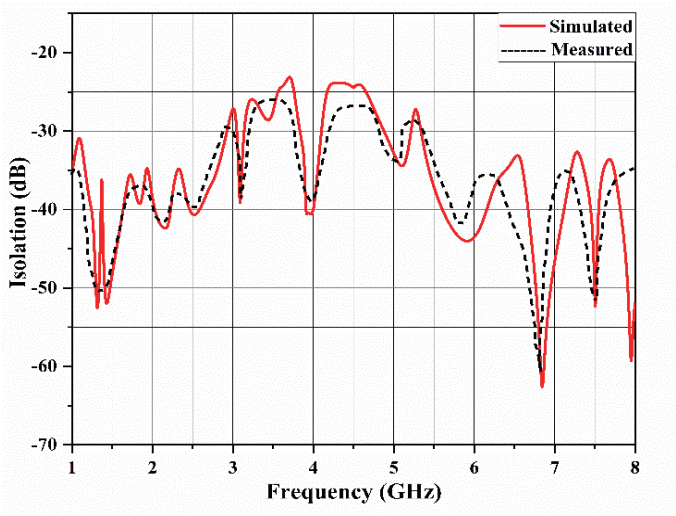

FIGURE 20. Simulated and measured S_{12} of the quad-element defected L-shaped microstrip patch MIMO antenna.

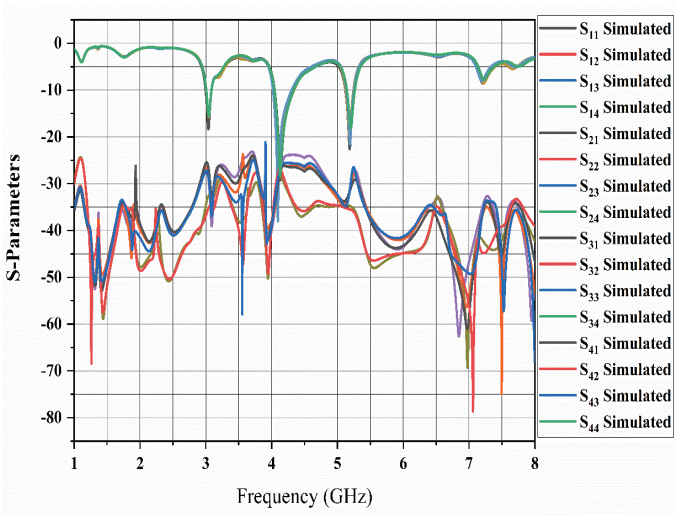

FIGURE 21. Simulated S-parameters of the quad-element defected L-shaped microstrip patch MIMO antenna.

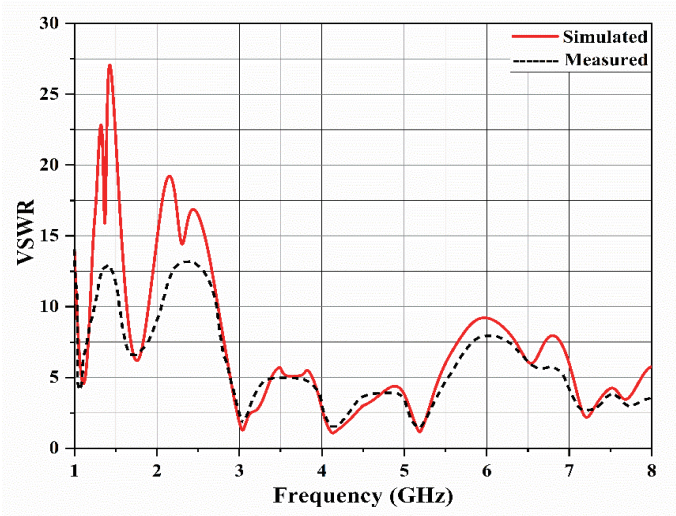

FIGURE 22. Simulated and measured VSWRs of the quad-element defected L-shaped microstrip patch MIMO antenna.

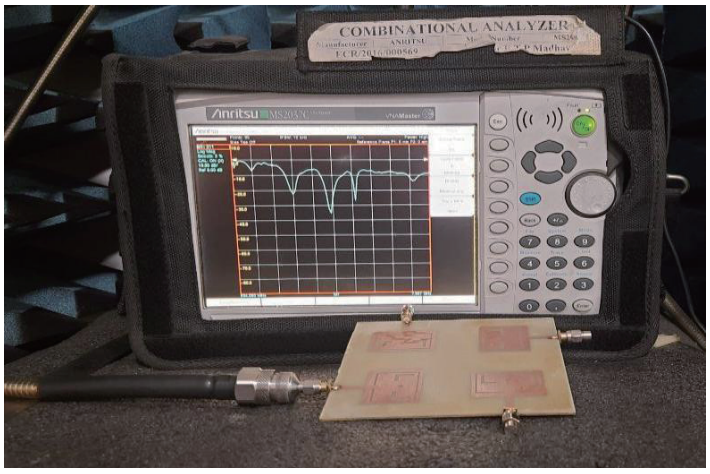

FIGURE 23. Measurement of S_{11} results by MS2037C anritsu combinational analyser.

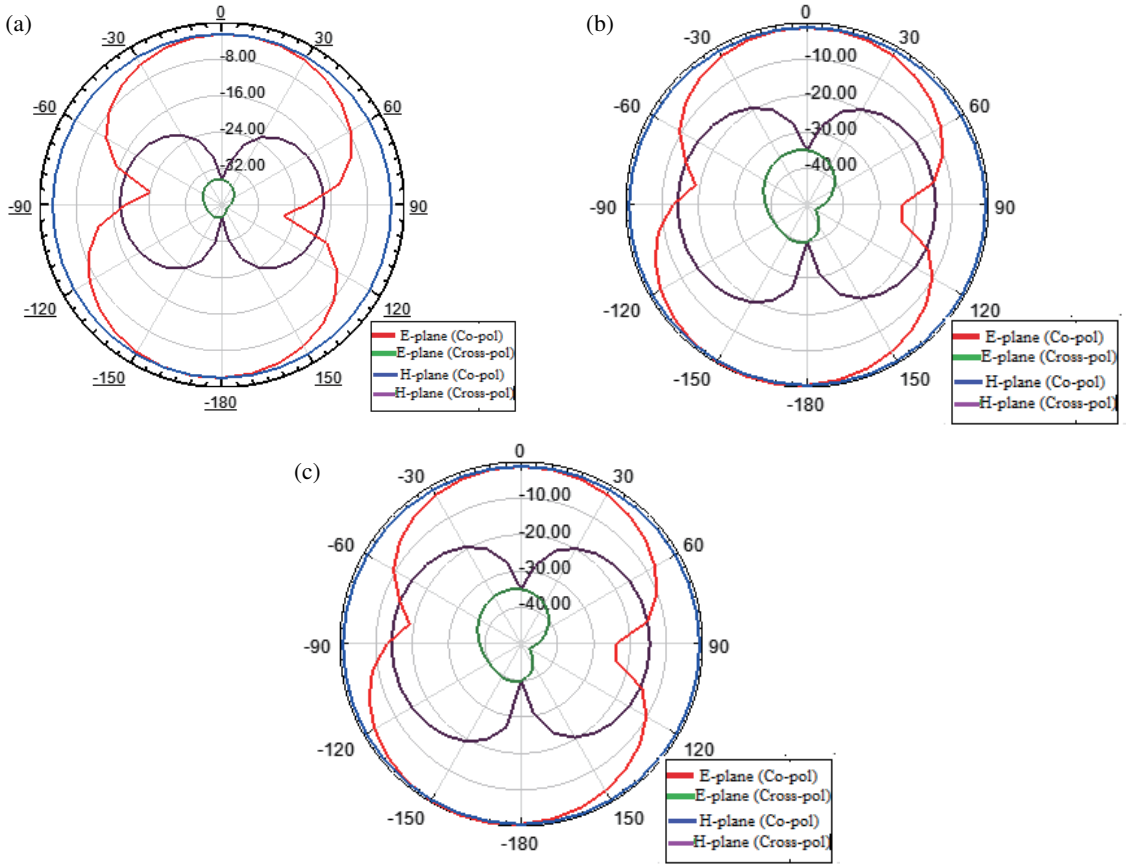

FIGURE 24. Simulated and measured radiation patterns of the quad-element defected L-shaped microstrip patch antenna (a) at 3 GHz (b) at 4.1 GHz (c) at 5.2 GHz.

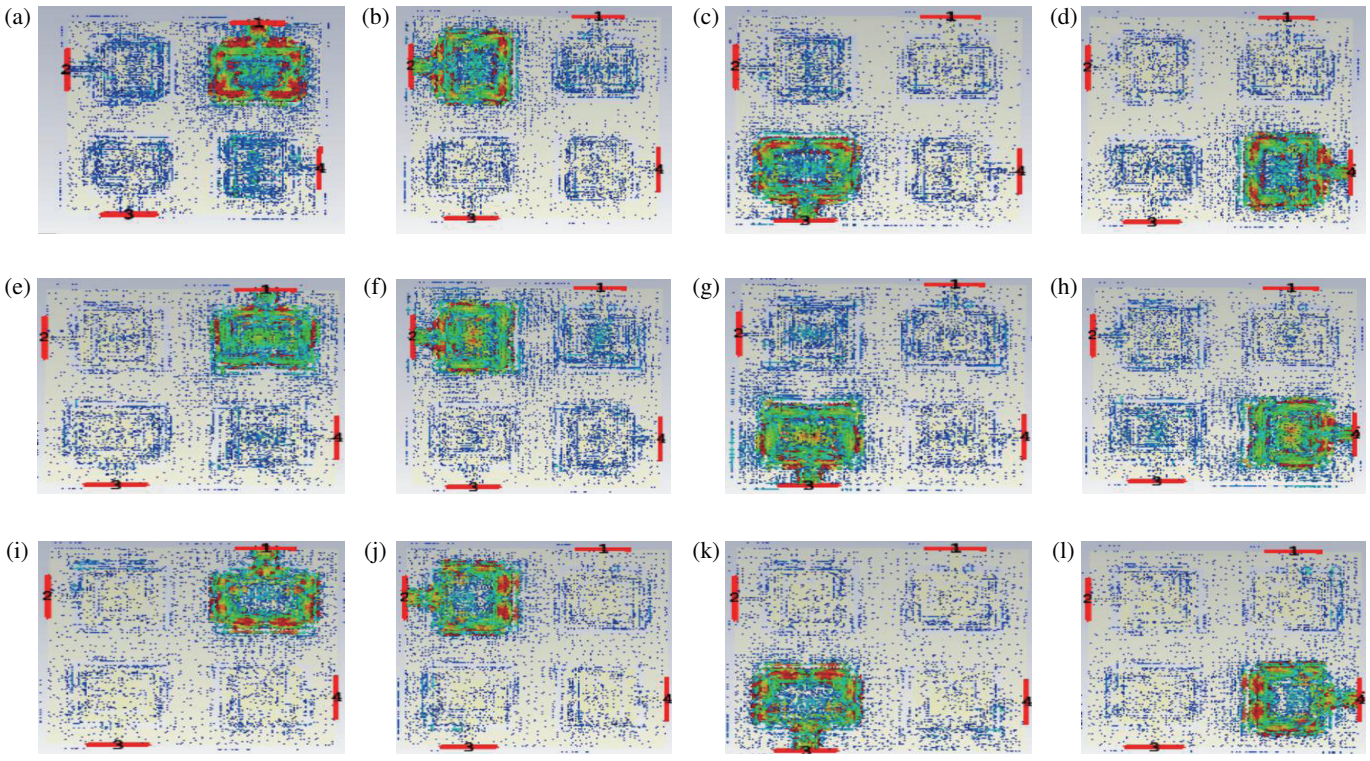

FIGURE 25. Surface current distribution of the dual-element defected L-shaped microstrip patch antenna (a)–(d) 3 GHz (e)–(h) 4.1 GHz (i)–(l) 5.2 GHz.

TABLE 2. The values of mean effective gain (MEG) at frequency sweep.

Operating Frequency (GHz)	1 Antenna	2 Antenna	3 Antenna	4 Antenna
1	6.986	6.454	7.733	7.1964
1.5	7.102	6.496	7.353	7.113
2	8.45	8.32	8.17	8.29
2.5	6.7986	6.4954	7.8733	7.0964
3	7.002	6.5496	7.1353	7.2113
3.5	6.961	6.6523	6.8876	7.0758
4	9.01	8.91	9.25	8.88
4.5	7.1013	8.20348	9.089	7.458
5	6.576	7.02412	7.630	7.0518
5.5	6.754	6.6025	7.359	6.6763
6	6.7986	6.4954	7.8733	7.0964

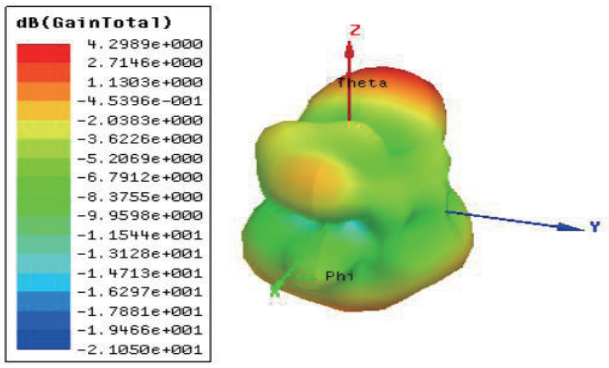

FIGURE 26. 3D gain of the quad-element defected hexagonal-patch MIMO antenna.

ECC is a significant parameter to access the performance of a MIMO antenna. It determines the correlation with the neighbouring elements present in the design. The typical value of ECC is 0, but it can range between the values of 0 to 0.5. It can be calculated in two ways either by using S-parameters or radiation pattern. This is a formula for ECC according to S-parameters

$$\rho_e = \frac{|S_{11}^* S_{12} + S_{21}^* S_{22}|^2}{(1 - |S_{11}|^2 - |S_{21}|^2)(1 - |S_{22}|^2 - |S_{12}|^2)}$$

$$ECC_{qp} = \frac{\left| \int_0^{2\pi} \int_0^{\pi} \left(E_{\theta p}^* E_{\theta q} P_\theta XPR + E_{\varphi p}^* E_{\varphi q} P_\varphi \right) d\Omega \right|^2}{\alpha \times \beta}$$

The above formula is for ECC as per the radiation pattern data.

$$\alpha = \int_0^{2\pi} \int_0^{\pi} \left(E_{\theta q}^* E_{\theta q} P_\theta XPR + E_{\varphi q}^* E_{\varphi q} P_\varphi \right) d\Omega$$

$$\beta = \int_0^{2\pi} \int_0^{\pi} \left(E_{\theta p}^* E_{\theta q} P_\theta XPR + E_{\varphi p}^* E_{\varphi q} P_\varphi \right) d\Omega$$

Diversity gain indicates the quality and reliability of a MIMO antenna. It is calculated by considering the values of ECC. Its ideal value should be 10 dB.

$$DG = 10 \times \sqrt{1 - |ECC_{qp}|^2}$$

Figure 27 illustrates the ECC and DG of dual-port MIMO antenna. The values of ECC and DG for this particular antenna meet the ideal ECC and DG values, indicating that the MIMO antenna is well suited for its intended purpose. From Figure 28, the simulated and measured values of ECC is at 3 GHz, 4.1 GHz and 5.2 GHz are below 0.5 which fulfils the ideal requirements of ECC of a MIMO antenna, and in Figure 29, the simulated and measured DG values of a MIMO antenna are at 10 dB.

The total active reflection coefficient can be used to evaluate the impedance bandwidth of an antenna by combining all the antenna elements. The TARC of the antenna model is evaluated by the TARC equation shown below. Figure 30 presents the TARC for a four-port L-shaped MIMO antenna. The equation shown below generates a curve by considering random values in the range between 0 and 2π.

$$S = Port$$

$$TARC = \sqrt{\frac{(S_{mn} + S_{mn})^2 + (S_{mn} + S_{mn})^2}{2}}$$

Mean effective gain is another useful metric to consider while the diversity of the antenna is calculated. It is referred as the ratio between the mean received power to the mean incident power. The MEG is calculated using the formula shown below. Since the MIMO antenna is constructed from identical antenna elements, there should not be a major difference in the gain achieved by different antenna components. The ideal theoretical limit for MEG is 0 dB. According to Table 2, the variance is within the permissible range, which makes the device more suitable for MIMO communications. The mean received power in a fading situation is the key parameter known as the mean effective gain. Table 2 shows the numbers calculated numerically. For good performance, the practical value suggested for the proposed antenna is -3 dB less than or equal to MEG

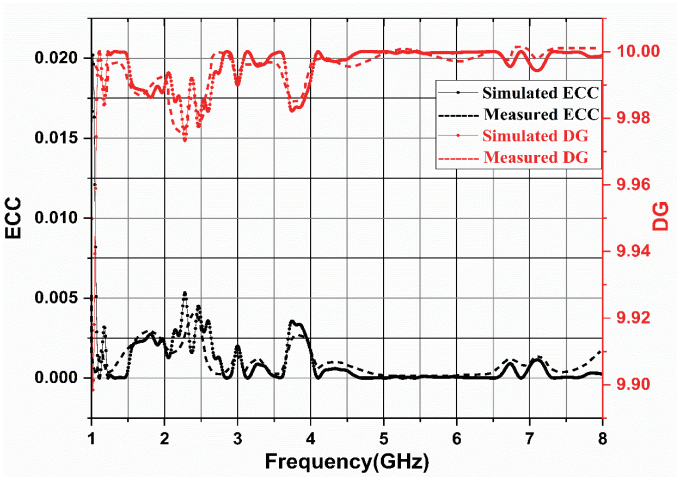

FIGURE 27. ECC and DG for dual-port MIMO antenna.

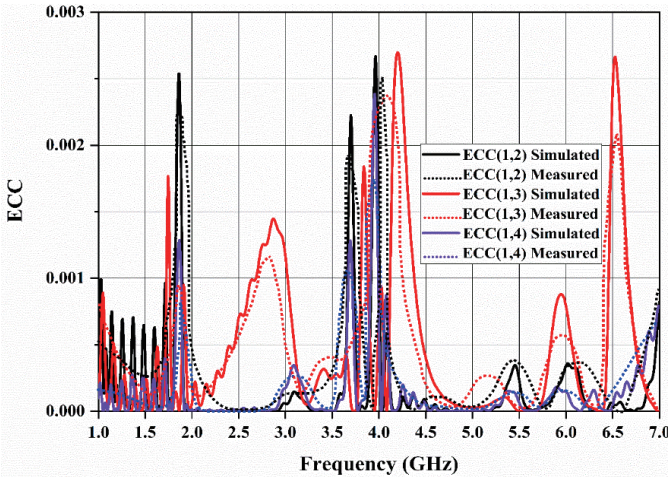

FIGURE 28. ECC of a four-port MIMO antenna.

TABLE 3. Comparison table of the proposed MIMO design to existing MIMO designs.

References	Element	Substrate	Bandwidth	Dimensions (mm^2)	Return Loss	Gain (dBi)	ECC	DG (dB)
[8]	4	FR4	3.5–4.2 GHz	140 × 140	< 20 dB	1.79–2.39	< 0.1	—
[9]	1	Polyamide	0.7–0.99 GHz 1.56–1.67 GHz 2.5–3.8 GHz 5–6 GHz 6–7 GHz	120 × 80	> 20 dB > 15 dB > 15 dB > 15 dB > 15 dB	——	——	——
	4	Polyamide	0.5–1.1 GHz 2.54–3.58 GHz 5.01–6.4 GHz 6.57–7.2 GHz	160 × 160	> 10 dB > 20 dB > 20 dB > 20 dB	−0.05 4.4 6.9 2.0	——	——
[10]	4	FR4	3.3–3.8 GHz 4.6–5.2 GHz	140 × 60	< −15 dB < −15 dB	2.7 1.5	< 0.001	—
[17]	1	FR4	3–10.5 GHz	50 × 50	> 20 dB	——	——	——
	2	FR4	3.5–11.8 GHz	80 × 40	> 20 dB	1.2–3.20	< 0.15	—
	4	FR4	3–12 GHz	80 × 80	> 20 dB	2 to 4	< 0.2	—
[18]	4	Rogers/RT Durid 5880	3–5.8 GHz	120 × 60	< −30 dB	1.8–3.25	0.016	> 9.9
[19]	4	FR4	3–6.2 GHz	125 × 125	< −10 dB	2.5–3.5	—	—
Proposed	**1**	FR4	3.04–3.09 GHz 4.11–4.13 GHz 5.18–5.21 GHz	60 × 60	−26.83 dB −20.06 dB −19.16 dB	2.5	—	
	2	FR4	3.04–3.09 GHz 4.11–4.13 GHz 5.18–5.21 GHz	60 × 120	−22.07 dB −40.09 dB −20.54 dB	3.1	< 0.014	9.99 9.99
	4	FR4	3.04–3.09 GHz 4.11–4.13 GHz 5.18–5.21 GHz	120 × 120	−18.36 dB −29.21 dB	4.2	< 0.003	9.99 9.99

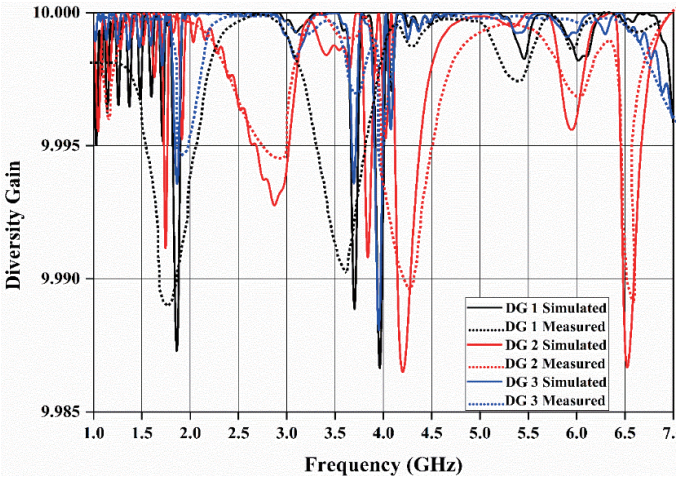

FIGURE 29. DG for four-port L-shaped MIMO antenna.

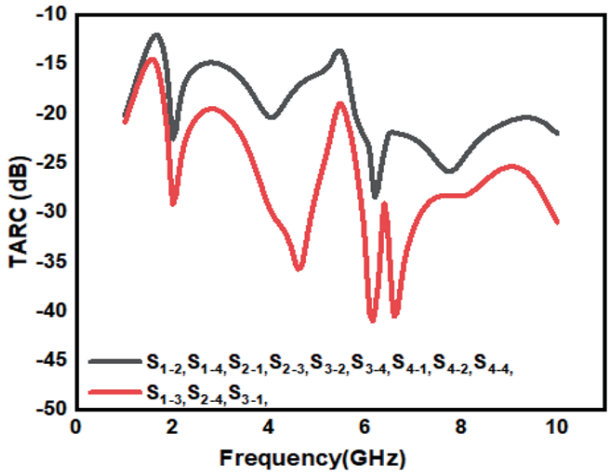

FIGURE 30. TARC for four-port L-shaped MIMO antenna.

(dB) −12. Thus, the MEG values of all MIMO configurations were verified.

$$MEG_i = 0.5\mu_{irad} = 0.5\left(1 - \sum_{j=1}^{K} \left|S_{ij}\right|\right) \quad (1)$$

where i = antenna under observation, μ = radiation efficiency.

Table 3 presents a comparison between the L-shaped MIMO antenna and various other MIMO antennas operating at sub-6 GHz. The comparison includes dimensions, return loss, gain, envelope correlation coefficient, and diversity gain. The proposed antenna is shown to outperform the other antennas in terms of size and performance. Previous articles [8–10, 17–19] have proposed MIMO antennas, but they are larger and provide less gain than the proposed antenna. Chemical etching of microstrip devices is a cost-effective way to improve manufacturing efficiency.

4. CONCLUSION

A quad-element MIMO antenna is proposed in this paper which describes in detail about the design of the antenna from a basic microstrip antenna to the proposed defected L-shaped microstrip patch MIMO through various modifications to resonate at the desired frequency. This proposed single antenna resonates at 3.0 GHz, 4.1 GHz, and 5.2 GHz frequencies with return loss −26.83 dB, −20.06 dB, and −19.16 dB, respectively. To improve the data rate, the existing design was modified to design both two- and four-port MIMO antennas. These antennas resonate at 3 GHz, 4.1 GHz, and 5.2 GHz with a return loss −22.07 dB, −40.09 dB, and −20.54 dB for two-port MIMO antenna and −18.35 dB, −29.21 dB, and −22.57 dB for four-port MIMO antenna. The antenna has an isolation of −27.16 dB at 3 GHz, −25.99 dB at 4.1 GHz, and −27.30 dB at 5.2 GHz for a four-element MIMO antenna, and for a two-port MIMO antenna at 3 GHz the isolation is −26.17 dB; at 4.1 GHz the isolation is −30.75 dB; and at 5.2 GHz the isolation is −27.80 dB. Along with S-parameters, MIMO diversity parameters like ECC is below 0.003, and DG is almost 10 dB. This design is useful for a variety of applications that require cellular communication, such as smart homes, industrial automation, agriculture, surveillance, and medical care.

REFERENCES

[1] Gong, Y., "Multiple input multiple out of smart antenna technology," *ZTE Technology*, Vol. 6, 19–21, 2002.

[2] Li, G. R. and M. Song, "MIMO technology in mobile communication," *Modern Telecommunication Technology*, Vol. 1, 42–45, 2004.

[3] Foschini, G. J., "Layered space-time architecture for wireless communication in a fading environment when using multi-element antennas," *Bell Labs Technical Journal*, Vol. 1, No. 2, 41–59, 1996.

[4] Foschini, G. J. and M. J. Gans, "On limits of wireless communications in a fading environment when using multiple antennas," *Wireless Personal Communications*, Vol. 6, 311–335, 1998.

[5] ITU-R, "IMT Vision—Framework and Overall Objectives of the Future Develop ment of IMT for 2020 and Beyond, document Recommendation ITU-R M.2083-0," 1–21, 2015.

[6] Kumar, S., A. S. Dixit, R. R. Malekar, H. D. Raut, and L. K. Shevada, "Fifth generation antennas: A comprehensive review of design and performance enhancement techniques," *IEEE Access*, Vol. 8, 163 568–163 593, 2020.

[7] Sarkar, D. and K. V. Srivastava, "Four element dual-band sub-6 GHz 5G MIMO antenna using SRR-loaded slot-loops," in *2018 5th IEEE Uttar Pradesh Section International Conference on Electrical, Electronics and Computer Engineering (UPCON)*, 1–5, Gorakhpur, India, 2018.

[8] Swindlehurst, A. L., E. Ayanoglu, P. Heydari, and F. Capolino, "Millimeter-wave massive MIMO: The next wireless revolution?" *IEEE Communications Magazine*, Vol. 52, No. 9, 56–62, Sep. 2014.

[9] Tuovinen, T., N. Tervo, and A. Pärssinen, "Analyzing 5G RF system performance and relation to link budget for directive MIMO," *IEEE Transactions on Antennas and Propagation*, Vol. 65, No. 12, 6636–6645, 2017.

[10] Paulraj, A. J., D. A. Gore, R. U. Nabar, and H. Bolcskei, "An overview of MIMO communications-a key to gigabit wireless," *Proceedings of the IEEE*, Vol. 92, No. 2, 198–218, 2004.

[11] Sharawi, M. S., *Printed MIMO Antenna Engineering*, Artech House, 2014.

[12] Jha, K. R., Z. A. P. Jibran, C. Singh, and S. K. Sharma, "4-port MIMO antenna using common radiator on a flexible substrate for sub-1 GHz, sub-6 GHz 5G NR, and Wi-Fi 6 applications," *IEEE Open Journal of Antennas and Propagation*, Vol. 2, 689–701, 2021.

[13] Barani, I. R. R. and K.-L. Wong, "Integrated inverted-F and open-slot antennas in the metal-framed smartphone for 2×2 LTE LB and 4×4 LTE M/HB MIMO operations," *IEEE Transactions on Antennas and Propagation*, Vol. 66, No. 10, 5004–5012, 2018.

[14] Liu, D. Q., M. Zhang, H. J. Luo, H. L. Wen, and J. Wang, "Dual-band platform-free PIFA for 5G MIMO application of mobile devices," *IEEE Transactions on Antennas and Propagation*, Vol. 66, No. 11, 6328–6333, 2018.

[15] Huang, J., G. Dong, J. Cai, H. Li, and G. Liu, "A quad-port dual-band MIMO antenna array for 5G smartphone applications," *Electronics*, Vol. 10, No. 5, 542, 2021.

[16] Srivastava, K., A. Kumar, B. K. Kanaujia, S. Dwari, and S. Kumar, "A CPW-fed UWB MIMO antenna with integrated GSM band and dual band notches," *International Journal of RF and Microwave Computer-Aided Engineering*, Vol. 29, No. 1, e21433, 2019.

[17] Karaboikis, M., C. Soras, G. Tsachtsiris, and V. Makios, "Compact dual-printed inverted-F antenna diversity systems for portable wireless devices," *IEEE Antennas and Wireless Propagation Letters*, Vol. 3, 9–14, 2004.

[18] Sharawi, M. S., A. B. Numan, and D. N. Aloi, "Isolation improvement in a dual-band dual-element MIMO antenna system using capacitively loaded loops," *Progress In Electromagnetics Research*, Vol. 134, 247–266, 2013.

[19] Yoo, S. and S. Kahng, "A compact MIMO antenna using ZOR split ring resonator radiators with a decoupling structure," *Microwave Journal*, Vol. 54, No. 11, S26–S31, Nov. 2022.

[20] Li, H., J. Xiong, Z. Ying, and S. He, "High isolation compact four-port MIMO antenna systems with built-in filters as isolation structure," in *Proceedings of the Fourth European Conference on Antennas and Propagation*, 1–4, 2010.

[21] Chou, H.-T., H.-C. Cheng, H.-T. Hsu, and L.-R. Kuo, "Investigations of isolation improvement techniques for multiple input multiple output (MIMO) WLAN portable terminal applications," *Progress In Electromagnetics Research*, Vol. 85, 349–366, 2008.

[22] Zhu, F., J. Xu, and Q. Xu, "Reduction of mutual coupling between closely-packed antenna elements using defected ground structure," in *2009 3rd IEEE International Symposium on Microwave, Antenna, Propagation and EMC Technologies for Wireless Communications*, 1–4, Beijing, China, 2009.

[23] Han, M.-S. and J. Choi, "Multiband MIMO antenna with a band stop filter for high isolation characteristics," in *2009 IEEE Antennas and Propagation Society International Symposium*, 1–4, North Charleston, SC, USA, 2009.

[24] Min, K.-S., D.-J. Kim, and Y.-M. Moon, "Improved MIMO antenna by mutual coupling suppression between elements," in *The European Conference on Wireless Technology*, 125–128, Paris, France, 2005.

[25] Hsu, C.-C., K.-H. Lin, H.-L. Su, H.-H. Lin, and C.-Y. Wu, "Design of MIMO antennas with strong isolation for portable applications," in *2009 IEEE Antennas and Propagation Society International Symposium*, 1–4, North Charleston, SC, USA, 2009.

[26] Lee, Y., H. Chung, J. Ha, and J. Choi, "Design of a MIMO antenna with improved isolation using meta-material," in *2011 International Workshop on Antenna Technology (iWAT)*, 231–234, Hong Kong, China, 2011.

[27] Sarabandi, K. and Y. J. Song, "Subwavelength radio repeater system utilizing miniaturized antennas and metamaterial channel isolator," *IEEE Transactions on Antennas and Propagation*, Vol. 59, No. 7, 2683–2690, 2011.

[28] Keriee, H., M. K. A. Rahim, O. Ayop, N. A. Nayyef, M. Ghanim, O. R. Alobaidi, B. Esmail, and Y. M. Hussein, "A slotted planar antenna for 5G applications," *ELEKTRIKA — Journal of Electrical Engineering*, Vol. 21, No. 2, 11–14, 2022.

[29] Thanuku, N., S. A. Kumar, and T. Shanmuganantham, "Design of 4-element MIMO antenna for ISM band applications," in *2019 IEEE Indian Conference on Antennas and Propogation (InCAP)*, 1–4, Ahmedabad, India, 2019.

[30] Parchin, N. O., Y. I. A. Al-Yasir, A. M. Abdulkhaleq, H. J. Basherlou, A. Ullah, and R. A. Abd-Alhameed, "A new broadband MIMO antenna system for sub 6 GHz 5G cellular communications," in *2020 14th European Conference on Antennas and Propagation (EuCAP)*, 1–4, Copenhagen, Denmark, 2020.

[31] Govardhani, I., M. V. Narayana, A. Navya, A. Venkatesh, S. C. Spurjeon, S. S. Venkat, and S. Sanjay, "Design of high directional crossed dipole antenna with metallic sheets for UHF and VHF applications," *International Journal of Engineering & Technology*, Vol. 7, No. 1.5, 42–50, 2017.

[32] Imamdi, G., M. V. Narayan, A. Navya, and A. Roja, "Reflector array antenna design at millimetric (mm) band for on the move applications," *ARPN Journal of Engineering and Applied Sciences*, Vol. 13, No. 1, 352–359, 2018.

[33] Immadi, G., M. V. Narayana, A. Navya, C. A. Varma, A. A. Reddy, A. M. Deepika, and K. Kavya, "Analysis of substrate integrated frequency selective surface antenna for IoT applications," *Indonesian Journal of Electrical Engineering and Computer Science*, Vol. 18, No. 2, 875–881, 2020.

[34] Reddy, K. H., M. V. Narayana, G. Immadi, P. Satyanarayana, K. Rajkamal, and A. Navya, "A low-profile electrically small antenna with a circular slot for global positioning system applications," *Progress In Electromagnetics Research C*, Vol. 133, 27–38, 2023.

[35] Rao, L. N., G. Immadi, M. R. Narayana, A. Navya, A. S. Madhuri, and K. Rajkamal, "A compact multiband hybrid rectangular DRA for wireless applications," *Progress In Electromagnetics Research Letters*, Vol. 117, 89–96, 2024.

[36] Majji, N. K., V. N. Madhavareddy, G. Immadi, N. Ambati, and S. M. Aovuthu, "Analysis of a compact electrically small antenna with SRR for RFID applications," *Engineering, Technology & Applied Science Research*, Vol. 14, No. 1, 12 457–12 463, Feb. 2024.

[37] Kumar, M. N., M. V. Narayana, G. Immadi, P. Satyanarayana, and A. Navya, "Analysis of a low-profile, dual band patch antenna for wireless applications," *AIMS Electronics and Electrical Engineering*, Vol. 7, No. 2, 171–186, 2023.

[38] Majji, N. K., V. N. Madhavareddy, G. Immadi, and N. Ambati, "A low-profile electrically small serrated rectangular patch antenna for RFID applications," *Engineering, Technology & Applied Science Research*, Vol. 14, No. 2, 13 611–13 616, Apr. 2024.

[39] Narayana, M. V., G. Immadi, A. Navya, M. V. Swathi, M. Nikhitha, B. Vineetha, and G. C. A. S. Swaroop, "Analysis of a quad port dual band MIMO antenna for sub-6 GHz applications," *Progress In Electromagnetics Research B*, Vol. 105, 137–151, 2024.